Eur. Phys. J. B **79**, 153–162 (2011)
DOI: 10.1140/epjb/e2010-10051-y

THE EUROPEAN PHYSICAL JOURNAL B

Regular Article

Investigation of $Cu_{0.5}Ni_{0.5}$/Nb interface transparency by using current-perpendicular-to-plane measurement

S.Y. Huang[1,2], J.J. Liang[3,a], S.Y. Hsu[2], L.K. Lin[1], T.C. Tsai[1], and S.F. Lee[1,b]

[1] Institute of Physics, Academia Sinica, 115 Taipei, Taiwan, Republic of China
[2] Institute of Electrophysics, National Chiao Tung University, 300 Hsinchu, Taiwan, Republic of China
[3] Department of Physics, Fu Jen University, 242 Taipei, Taiwan, Republic of China

Received 18 January 2010 / Received in final form 22 June 2010
Published online 6 January 2011 –

Abstract. A direct determination of the interfacial transparency on the basis of current-perpendicular-to-plane (CPP) resistances for $Cu_{0.5}Ni_{0.5}$/Nb layered system is presented. This particular realization has substantial significance for understanding the interfacial transport in such heterostructures. The unexpected large critical thickness for this weak ferromagnetic containing system can be attributed to the strong pair-breaking effect as a result of the high interfacial transparency. Besides, the strong pair-breaking also plays a decisive role in the occurrence of the dimensionality crossover of the temperature dependent upper critical magnetic field.

1 Introduction

Surface and interface related phenomena are important in nano science and technology. The proximity effect between a ferromagnet (F) and a superconductor (S) has attracted tremendous attention for several decades [1]. Extensive works have been devoted to the study of the coexistence of ferromagnetism and superconductivity at the junction of a ferromagnet and a superconductor in layered systems, such as Gd/Nb and Co/Nb multilayers, Ni/Nb bilayers, and Fe/V/Fe trilayers [1]. The controversy in such systems is that the exchange field in the ferromagnet is expected to break the time-reversal symmetry in the superconductor and suppress singlet superconductivity. While superconductor prefers an antiparallel spin orientation to form Cooper pairs, the ordered ferromagnet forces the spins to align in parallel. Because superconductivity and ferromagnetism are two competing orders, their coexistence, known as the LOFF state, is possible only in a narrow interval in phase space [1–3]. Upon entering the ferromagnet, the superconducting order parameter exhibits spatial variation due to energy shift between the constituents of the quasiparticle in the presence of the exchange field. As a consequence, the superconducting wavefunction not only decays in the F layer but also oscillates over a certain length in the direction perpendicular to the interface. Interesting effects, such as the F layer thickness (d_F) dependent nonmonotonic oscillating superconducting critical temperature (T_c) [4,5] and critical current (I_c) [6–8], and the reentrant superconducting behavior emerge in F/S layered structures [9,10]. Over recent years, advances in the fabrication of artificial F/S layered structures have enabled the study of these effects from both the fundamental and the applicative aspects when the two orders are spatially separated. To reliably control F thickness over a large range in $S/F/S$ junction, it is essential to use a weak ferromagnetic metal [6,7]. For the study of quasiparticles-mediated coupling in the $F/S/F$ spin valve structure, a thin S layer is required [11–13].

The quality of the interface is important for understanding the coupling mechanism between the S and the F. Lately, interfacial transparency T_{tran}, has been taken into consideration in the analysis of the interfacial quality and is considered to play a dominant role in the boundary condition in layered structures [13–20]. While $T_{tran} = 1$ indicates a perfect interface, the values of $T_{tran} < 1$ signifies the decrease in the amplitude of the order parameter. It follows that electrons are apt to be reflected rather than transmitted at the interfaces, which may reduce the strength of the proximity effect [14,15]. It is known that the reduced transparency may result from both extrinsic and intrinsic factors such as interface imperfection, Fermi velocities difference, and band-structures mismatch. By considering the interfacial transmission coefficient in the proximity theory, the discrepancy between the experimental results and the theoretical prediction under a perfect interface assumption could be reconciled. Attanasio et al. have studied interfacial transparency for different layered structures, which consist of Nb as a superconductor, Cu, Ag, and Pd as normal metals, and PdNi

[a] e-mail: phys2021@mails.fju.edu.tw
[b] e-mail: leesf@phys.sinica.edu.tw

and Fe as ferromagnetic materials, trying to correlate the effect of the fabrication method to T_{tran} with sputtering and molecular beam epitaxy. Their results showed that the interfacial transparency was influenced mainly by the intrinsic factors related to the microscopic properties of the two metals across the interface rather than by the fabrication method [16]. Although interfacial transparency is important both from the theoretical and experimental points of view, it has been hitherto treated as a fitting parameter due to the great difficulty in direct measurement [13–20].

In the present work, we report a systematic investigation of the current perpendicular to plane (CPP) resistance and T_c in dependence of the thickness for $Cu_{0.5}Ni_{0.5}$/Nb layered structures, aiming at the transport characteristics at the interface. Unit area resistances for one pair of interfaces are deduced by a series resistor model from the CPP measurements. Together with the results of the superconducting critical temperature as a function of individual layer thickness, we are able to determine the interfacial transparency between the S and the F quantitatively. High interfacial transparency in this system is obtained. From the study of the dimensionality crossover, it reveals that high interfacial transparency significantly influences the behavior of the temperature dependence of the critical magnetic field (H_{c2}) through the strong pair-breaking effect. This paper is organized as follows. Section 2 contains a brief description of the sample preparation and characterization. In Section 3, the CPP measurements and the interface resistance studies are presented. In Section 4, the critical temperature is studied based on the solutions of the Usadel equations subject to the boundary conditions developed by Fominov [15]. The determination of interfacial transparency is demonstrated. In Section 5, the two-dimensional (2D) to three-dimensional (3D) crossover in superconductors and the strength of the pair-breaking effect is discussed from the temperature-dependent H_{c2} measurements. Finally, a summary is presented in Section 6.

2 Sample preparation and characterization

The samples were grown on Si (100) substrates in a magnetron sputtering system with a base pressure of less than 2×10^{-7} torr. Highly pure Ar gas (99.999%) used was further purified by passing through a liquid N_2 cold trap. To minimize the variations in the preparatory condition and obtain comparable physical quality for a specific set, by using a movable substrate holder, we could fabricate 12 samples for current in the plane (CIP) configurations in the same deposition run but 8 samples for CPP configurations in another same deposition run. The growth of the CIP samples was less complicated than that of the CPP ones, in which three contact masks must be changed in situ to ensure clean interfaces. The deposition conditions used for the CPP samples were similar to those used for studying the Co/Nb_xTi_{1-x} multilayers reported earlier [21]. The sample was deposited at room temperature

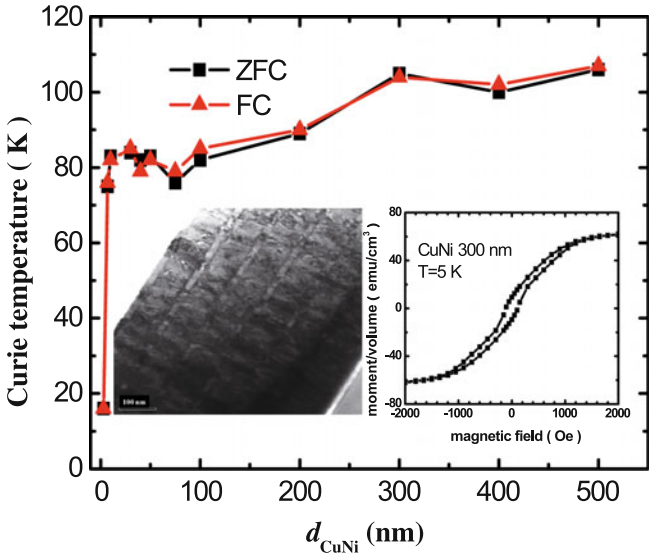

Fig. 1. (Color online) Curie temperature versus $Cu_{0.5}Ni_{0.5}$ layer thickness with zero field cool (square) and field cool (triangle) methods. The solid lines are the guide to eye. Right inset: magnetic hysteresis loop for $Cu_{0.5}Ni_{0.5}$ thickness of 300 nm at $T = 5$ K. Left inset: the TEM cross-section image of the sample of [$Cu_{0.5}Ni_{0.5}$ 20 nm/ Nb 100 nm]$_6$/ $Cu_{0.5}Ni_{0.5}$ 20 nm multilayer.

by sputtering. Ex situ X-ray diffraction showed crystalline structures of bcc (100) for Nb and fcc (111) for CuNi.

According to the binary phase diagrams, Cu and Ni can form alloys at room temperature. The Ni concentration was $50 \pm 1\%$ analyzed by energy dispersive X-ray analysis (EDX). The formation of Ni-rich atomic clusters near the composition $Ni_{0.5}Cu_{0.5}$ gives rise to magnetic clusters. The spin moment of $Cu_{0.5}Ni_{0.5}$ alloys on a Ni atom depended on the local atomic environment which is specified by the number of Ni nearest neighbor and the number of Ni second nearest neighbors [22]. The existence of cluster was studied by the width of the peak which reflected the size of spin cluster in neutron-scattering measurements [23]. However, the detail of local structure around Ni atoms in $Cu_{0.5}Ni_{0.5}$ alloy will require further experiments probed by the extended X-ray absorption fine structure (EXAFS) technique. To characterize the properties of the F films, magnetic moment measurement was performed on a series of $Cu_{0.5}Ni_{0.5}$ single layers using a commercial SQUID magnetometer with magnetic fields applied parallel to the sample surface. Figure 1 shows the Curie temperature, T_{Curie}, versus the $Cu_{0.5}Ni_{0.5}$ thickness, which is derived from the temperature dependence of the magnetization, M, with field-cooled and zero-field-cooled measurement at 30 Oe. The T_{Curie} is about 80−110 K in agreement with the results reported for bulk samples at this composition [24]. The saturation magnetization, M_{sat}, of $Cu_{0.5}Ni_{0.5}$ calculated from the hysteresis loop at 5 K (see the right inset of Fig. 1) is about 0.1 μ_B/atom. There is no clear indication of the thickness dependence of T_{Curie} and M_{sat} as d_{CuNi} is larger than 7 nm.

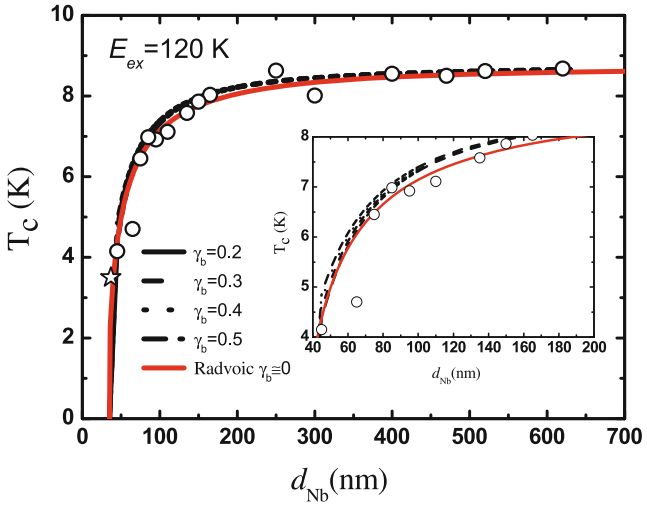

Fig. 2. (Color online) Superconducting critical temperatures as a function of d_{Nb} for $Cu_{0.5}Ni_{0.5}$/Nb/$Cu_{0.5}Ni_{0.5}$ trilayers with constant $Cu_{0.5}Ni_{0.5}$ thickness $d_{\mathrm{CuNi}} = 50$ nm. The solid (red) line is the fitting with high interfacial transparency assumption. The other lines are calculated with various values of γ_b. $E_{ex} = 120$ K is chosen after Figure 3. The inset is an enlargement of the region between 40 nm and 160 nm close to the corner. The star symbol represented T_c for the asymptote of CuNi thickness in the set of $d$$Cu_{0.5}Ni_{0.5}$/Nb/$d$$Cu_{0.5}Ni_{0.5}$ trilayers.

The superconducting critical temperature and critical field are resistively measured in a ^{4}He cryostat by a standard four-probe technique. The geometry for these CIP samples is 5 mm long and 1 mm wide between the voltage contact pads. The definition of T_c was taken at the temperature corresponding to 90% of the normal resistance. Figure 2 shows the dependence of T_c on the thickness of the Nb layer for $Cu_{0.5}Ni_{0.5}$/Nb/$Cu_{0.5}Ni_{0.5}$ trilayers with d_{CuNi} fixed at 50 nm. A monotonically rapid decline in T_c with decreasing d_{Nb} results from the depression of the amplitude of the superconducting wavefunction, induced by the pair-breaking effect near the F/S interface. The superconducting transition can be recorded down to the base temperature 1.7 K of our cryostat. Based on the weak ferromagnetic nature of $Cu_{0.5}Ni_{0.5}$ ascertained by magnetic measurement and the good quality of the interface verified by the transmission electron microscopy (TEM) image shown in the left inset of Figure 1, the solid line in Figure 2 can be fitted by a model developed by Radovic et al. under the assumption of a perfect interface [25]. Detailed discussion of this subject has been reported in reference [26]. The critical thickness d_{crit} extrapolated from the fitting cure to $T_c = 0$ is determined to be 35 nm. Compared with the strong ferromagnet, in which d_{crit} is 30 nm for Co/Nb/Co [27] and 34 nm for Fe/Nb/Fe [28], the critical thickness of 35 nm for $Cu_{0.5}Ni_{0.5}$/Nb/$Cu_{0.5}Ni_{0.5}$ is unexpectedly large regarding the weak exchange field. The critical thickness in our system is larger than not only strong ferromagnet but even for the weak ferromagnet CuNi system in previous reports. In principle, the order parameter induced by a superconductor in ferromagnet results in an oscillation of the critical temperature for increasing F layer thickness in S/F bilayers. Sidorenko et al. observe oscillation reentrant behavior for Nb = 7.8 and 7.3 nm, respectively, in Nb/$Cu_{0.41}Ni_{0.59}$ bilayers. When Nb was increased to 14.1 nm, the T_c oscillation was flat with a shallow minimum [29]. Rusanov et al. report the critical thickness is about 18 nm in $Cu_{0.41}Ni_{0.59}$/Nb/$Cu_{0.41}Ni_{0.59}$ trilayers system. However, the dip in $T_c(dF)$ of Nb/$Cu_{0.41}Ni_{0.59}$ bilayers with dNb = 18 nm was very small. They mentioned that the absence of dips may probably due to the interfaces less than fully transparent [30]. In this report, we demonstrate that a strong pair breaking effect can be induced at the interface between $Cu_{0.5}Ni_{0.5}$ and Nb. The interfacial transparency between two metals with different Fermi energies is a quantum mechanical problem of reflection and transmission of charge carriers at the interface [31]. This mismatch of the Fermi wavevector may reduce the transmission across the interface, especially a comparison between the Cooper pair with opposite spins in a superconductor and the Fermi momentum of the energy-split subbands in a ferromagnet. By using CPP measurement, the transport properties of the interface between F and S can be quantitatively characterized.

3 CPP measurement

To quantitatively analyze the interface resistance in the superconducting and normal states, two sets of samples with different numbers of bilayers were fabricated. The measurements were carried out at 4.2 K. The thickness of $Cu_{0.5}Ni_{0.5}$ was fixed at 50 nm. The thicknesses of Nb were chosen respectively as 15 and 80 nm according to the phase diagram of Figure 2. The 15 nm Nb thickness was thinner than the critical thickness, it was in the normal state (NM) and the samples were F/NM multilayers. On the contrary, samples consisting of 80 nm Nb formed F/S multilayers. In Figure 3, we plotted the product of sample area A and total resistance R_T versus bilayer number N for the two series of $Cu_{0.5}Ni_{0.5}$/Nb multilayers. In the CPP geometry, AR_T is the unit area resistance since all areas conduct in parallel. As can been seen in Figure 3, AR_T is linearly proportional to the number of bilayers for both sets of samples. No magnetoresistance was observed on these samples. The fact that the resistance remains the same while an external magnetic field was applied implies that the spin-up and spin-down electron channels could not be distinguished. Therefore, we infer that there is strong spin mixing at the $Cu_{0.5}Ni_{0.5}$/Nb interface and/or in the Nb layer [32,33]. The linear behavior of AR_T versus N can be described by a one-band series resistance model expressed as [34]

$$AR_T = 2AR_{F/S(S)} + \rho_F t_F + N\left(\rho_F t_F + \rho_S t_S + 2AR_{F/S(NM)}\right) \quad (1)$$

for normal state Nb and

$$AR_T = 2AR_{F/S(S)} + \rho_F t_F + N\left(\rho_F t_F + 2AR_{F/S(S)}\right) \quad (2)$$

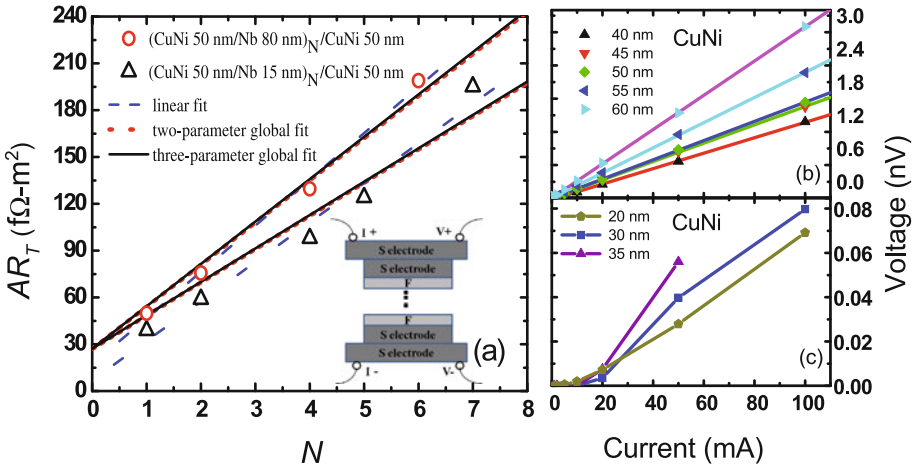

Fig. 3. (Color online) (a) Unit area resistance, AR_T, versus bilayer number N measured at 4.2 K. The two sets of samples have Nb thickness of 80 nm and 15 nm, respectively. The dashed lines are the linear least squares fit to the data. The dotted lines and the solid lines are the global fits to the data with two and three parameters, respectively. Inset: schematic cross section of CPP miltilayers sample. (b) Linear $I-V$ characteristic as a function of $Cu_{0.5}Ni_{0.5}$ thickness for CPP $Cu_{0.5}Ni_{0.5}$/Nb multilayer. The solid lines are the linear least squares fit to the data. (c) Non-linear $I-V$ characteristic as a function of $Cu_{0.5}Ni_{0.5}$ thickness for CPP $Cu_{0.5}Ni_{0.5}$/Nb multilayer. The solid lines are the guide to the eye.

for superconducting state Nb. Here, t's are the corresponding layer thicknesses, ρ's are the resistivities, $AR_{F/S(NM)}$'s are the unit area interface resistances between normal state Nb and $Cu_{0.5}Ni_{0.5}$ layers, and $AR_{F/S(S)}$'s are the unit area interface resistances between the superconducting state Nb and $Cu_{0.5}Ni_{0.5}$ layers. Recently, theoretical research asserted that the asymmetry of interface transparency in the $F/S/F$ structure originates mainly from the unequal interfacial transparencies of the F/S and S/F. This asymmetry can be observed from the T_c dependence on the relative magnetization orientation between two adjacent ferromagnetic layers by varying the F thicknesses in the $F1/S/F2$ structure [35]. Though we assume the interface resistances are identical on the ground of the same F thickness in all of the CPP multilayer samples, we use the notation $2AR_{F/S(NM)}$ and $2AR_{F/S(S)}$ for every pair of interfaces in equations (1) and (2), respectively. In Figure 3a, the dashed lines are the linear least squares fits to individual sets of data. According to the one-band model, equations (1) and (2) can be neatly expressed by $AR_T = C_1 + C_2N$ and $AR_T = C_1(N+1)$ for the normal and superconducting states of Nb, respectively, where $C_1 = 2AR_{F/S(S)} + \rho_F t_F$ and $C_2 = 2AR_{F/S(NM)} + \rho_F t_F + \rho_S t_S$. AR_T for each series of samples can be individually fitted with the model. In this manner, however, the same quantities deduced from the fitting are sample series dependent. To overcome this difficulty, a global fit was performed to analyze the two sets of data with the same fitting parameters. The results of the two-parameter global fit are shown in Figure 3a as dotted lines. In principle, we could use independently measured CuNi and Nb resistivities to get the interface resistances. However, when the CuNi thicknesses were varied, we found that the supercurrent penetrating into the CuNi layers played an important role in deriving the interface resistance.

As shown in Figures 3b and 3c, non-linear $I-V$ behavior was observed when the thickness of $Cu_{0.5}Ni_{0.5}$ was less than 40 nm. The voltage drop across the sample in the CPP measurements was less than 10 nV for a maximum current of 100 mA that was provided by a battery-powered DC current source. This voltage is six orders of magnitude smaller than the energy gap of 1.4 meV for Nb. Under these circumstances, the measured non-linear $I-V$ curve can be attributed to the presence of a supercurrent in the F layer. The $S/F/S$ structure can be regarded as a Josephson junction in that the superconductor couples weakly through the ferromagnetic barrier. It has been shown that the critical current of the ferromagnetic Josephson junction, I_{Jc}, will change signs from positive to negative under certain conditions, corresponding to a phase shift between two S layers in the Josephson ground state [1]. This phase change in the Cooper pair wavefunction is induced in the F layer by the proximity effect. As has been reported, I_{Jc} exhibited a non-linear IV characteristic, even for the thickness of the ferromagnet larger than the diffusion length of the Cooper pairs in the F layer, ξ_F^*. The largest spacer layer presented in the literature was 28 nm for CuNi [6,7], 11 nm for Ni, and 5 nm for Co [8]. The non-linear IV-characteristic could be well described by the expression $V = R_{NM}\sqrt{I^2 - I_{Jc}^2}$ because a supercurrent can be sustained even through a ferromagnet. Here, I_{Jc} was taken at the point where the $dV/dI(V)$ increased above the value of the zero bias current. R_{NM} was measured by applying a sufficient large bias current so that the nonlinear part of the current voltage curves could be ignored. Yet, the current was kept small enough to ensure the Nb electrodes remained in the superconducting state.

To characterize the average penetration depth of the supercurrent from the Nb layer into the $Cu_{0.5}Ni_{0.5}$ layer, we introduce a leakage length, δ_S. By fitting the data

in the ohmic region, we found that $\delta_S \approx 15.8$ nm. The long-range supercurrent may be due to spin-triplet pair correlations, which have been predicted to occur at the interface between a conventional spin-singlet superconductor and a ferromagnet in the presence of certain types of magnetic inhomogeneity. There has been at least one report of a Josephson current in $S/F/S$ structures using half metallic CrO_2 as the F material, where the distance between the S layers was several hundred nm [36]. According to theoretical work, spin-triplet correlations could be generated if the Cooper pairs experience regions of noncollinear magnetization [37,38]. For example, the neighboring domains have antiparallel magnetization, the long-range triplet component is generated in the domain walls. Recently, the domain size of $Cu_{0.47}Ni_{0.53}$ has been measured to be about 100 nm by high-resolution Bitter decoration technique below the Curie temperature (∼60 K) [39], which is not so different from the Nb coherence length. More recently, Khaire et al. observed a long-rang supercurrent in Josephson junctions containing Co in the range of 12−28 nm, when thin layers of either PdNi or CuNi weak ferromagnetic alloys were inserted [40]. This leakage length should be included in the above model. Accordingly, equations (1) and (2) are revised to be

$$AR_T = 2AR_{F/S(S)} + \rho_F t_F - 2\delta_S\rho_F + N\left(\rho_F t_F + \rho_S t_S + 2AR_{F/S(NM)}\right) \quad (3)$$

for the normal state and

$$AR_T = 2AR_{F/S(S)} + \rho_F t_F - 2\delta_S\rho_F + N\left(\rho_F t_F + 2AR_{F/S(S)} - 2\delta_S\rho_F\right) \quad (4)$$

for the superconducting state. They account for the fact that $Cu_{0.5}Ni_{0.5}$ contributes no resistance within the leakage length. From the results of the two-parameter global fit, the resistance of one-pair interfaces can be obtained by substituting the values of the bulk resistivities of Nb and $Cu_{0.5}Ni_{0.5}$ into equations (3) and (4). However, the uncertainty about the deduced interface resistance is found to be dominated by the large resistivity of the $Cu_{0.5}Ni_{0.5}$ alloy. To get more accurate results, the CPP resistivity measurement is carried out by varying the thickness of a single $Cu_{0.5}Ni_{0.5}$ film sandwiched between two Nb strips. The top view geometry for the measurement is illustrated in the inset of Figure 4. The effective area is confined to the overlapped square of the strips [41,42]. As shown in Figure 4, the unit area CPP resistance is linearly proportional to the thickness of the $Cu_{0.5}Ni_{0.5}$ layer. The individual linear least squares fit yields a slope associated with the CPP resistivity $\rho_{CuNi} = 380 \pm 20$ nΩ m. This linear behavior can be described by the one-band series-resistor model given by

$$AR_T = 2AR_{F/S(S)} + \rho_F\left(t_F - 2\delta_S\right). \quad (5)$$

Putting in $\rho_{CuNi} = 380 \pm 20$ nΩ m and independently measured $\rho_{Nb} = 80 \pm 8$ nΩ m, we obtain $2AR_{CuNi/Nb(S)} = 19.8 \pm 0.5$ fΩ m^2 and $2AR_{CuNi/Nb(NM)} = 0.6 \pm 0.1$ fΩ m^2. Finally, we performed a three-parameter global fit to all

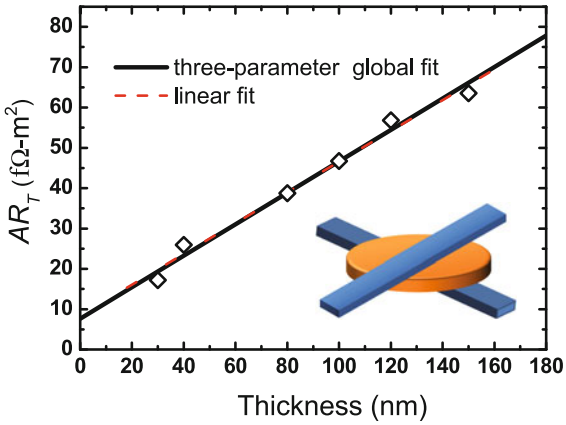

Fig. 4. (Color online) Unit area resistance, AR_T, versus $Cu_{0.5}Ni_{0.5}$ thickness measured at 4.2 K. The dashed line is the result of the linear least squares fit and the solid line is that of the global fit with three parameters. Also shown is the top view geometry of the current perpendicular to plane configuration for this series sample. Single CuNi film is sandwiched between two superconducting electrodes of Nb stripes used for the four-point measurement.

three data sets with the same set of parameters. The results are the best global fit solid lines in Figures 3a and 4 with $\rho_{CuNi} = 390 \pm 10$ nΩ m, $2AR_{CuNi/Nb(S)} = 19.9 \pm 1.5$ fΩ m^2, and $2AR_{CuNi/Nb(NM)} = 0.7 \pm 0.2$ fΩ m^2.

It is of particular interest to know how the interface resistance changes when the S becomes superconductive. The opening of the superconducting gap, Δ, at the Fermi energy and the decrease in population of quasiparticles make the S a low carrier system for spin transport. However, current can flow through the sample in response to a voltage smaller than Δ/e by virtue of the Andreev reflection in the metallic junction. For instance, a spin-up electron injected from a normal metal is retroreflected at the interface as a spin-down hole in order to form a Cooper pair in the superconductor [43]. On the other hand, exchange splitting of the conduction band in the F would suppress the Andreev current at the F/S interface and leads to the necessity of the spinless current inside the S [32]. Furthermore, the spin accumulation and spin-flipping scattering at the interface bring about an additional voltage drop across the interface and a reduction of spin transport into the S [44]. These could be the main factors responsible for the larger interface resistance of $Cu_{0.5}Ni_{0.5}$/Nb in the superconducting state than in the normal state. Since the individual effect on interface resistance cannot be differentiated based on the results obtained here, a quantitative analysis of the distinctive contribution to interface resistance is beyond the scope of this work.

4 Nonmonotonic critical temperature analysis by proximity effect theory

To study the behavior of both $T_c(d_S)$ and $T_c(d_F)$ we adopt a model developed by Fominov et al. [15] and extend it

to be applicable to trilayer systems. In the dirty limit, the critical temperature of a superconductor embedded between two ferromagnetic layers was calculated from the linearized Usadel equation. The anomalous functions F_S and F_F in the S and F layers, integrated over energy and averaged over the Fermi surface, are connected with the quasiclassical propagation boundary conditions near the interfaces. Within the single-mode approximation, the critical temperature can be obtained by solving the following equation:

$$\ln\left(\frac{T_{cS}}{T_c}\right) = \psi\left(\frac{1}{2} + \frac{\Omega_0^2}{2}\frac{T_{cS}}{T_c}\right) - \psi\left(\frac{1}{2}\right), \tag{6}$$

where ψ is the digamma function and T_{cS} is the bulk critical temperature. Ω_0, given later in this section, can be derived from the boundary conditions by matching the pairing function at the interface between S and F, as given by Kupriyanov and Lukichev [45]:

$$\xi_S \left.\frac{dF_S}{dx}\right|_{If} = \gamma\xi_F^* \left.\frac{dF_F}{dx}\right|_{If}, \quad \gamma = \left.\frac{\rho_S\xi_S}{\rho_F\xi_F^*}\right|_{If}, \tag{7}$$

$$\xi_F^*\gamma_b \left.\frac{dF_F}{dx}\right|_{If} = [F_S(0) - F_F(0)]|_{If}, \quad \gamma_b = \left.\frac{AR_b}{\rho_F\xi_F^*}\right|_{If}. \tag{8}$$

Here, ξ_S is the superconductor coherence length, while ξ_F^* is a spatial scale related to the diffusive motion of the Cooper pair in the F layer without considering the exchange field and is defined as

$$\xi_F^* = \sqrt{\frac{\hbar D_F}{2\pi k_B T_{cS}}}, \tag{9}$$

where k_B is the Boltzmann constant. The diffusion constant D_F can be estimated in terms of the mean free path and the Fermi velocity. Furthermore, the diffusion constant is related to low temperature resistivity of F, ρ_F, and the coefficient of electronic specific heat, γ_F, following the relationship $D_F = v_F\ell/3 = 1/(3\gamma_F\rho_F)(\pi k_B/e)^2$. The physical meaning of γ in equation (7) is the strength of the proximity effect between the F and S metals. It is essential to note that the Radovic's model adopts a boundary condition of high-quantum-mechanical transparency at the F/S interface, so the pairing function varies continuously at the interface, as indicated by $F_S = F_F$ [25]. In the present work, the boundary condition implies a jump of the pairing function depending on the magnitude of γ_b in equation (8). Furthermore, the boundary conditions at the outer surfaces are $\left.\frac{dF_S}{dx}\right|_{os} = \left.\frac{dF_F}{dx}\right|_{os} = 0$, accounting for the absence of the pairing function current through the outer surface of the trilayer. The Usadel equation in the F layer is readily solved, $F_F = C(\omega_n)\cosh(k_F[x + d_F])$. At the boundary $x = 0$, it is related to F_S from $\frac{dF_S(0)}{dx} = \frac{\gamma}{\gamma_b + B_F(\omega_n)}F_S(0)$ with the Mosubara frequency ω_n. In the single-mode approximation, T_c as a function of d_S and d_F for the $F/S/F$ trilayer systems takes the following form:

$$\Omega_0 \tan\left(\Omega_0\frac{d_S}{2\xi_S}\right) = \gamma\frac{A_S\left(\gamma_b + \mathrm{Re}B_F\right) + \gamma}{A_S\left|\gamma_b + B_F\right|^2 + \gamma\left(\gamma_b + \mathrm{Re}B_F\right)}$$

with

$$B_F = \left[k_F\xi_F^*\tanh(k_F d_F\right]^{-1},$$

$$k_F = \frac{1}{\xi_F^*}\sqrt{\frac{|\omega_n| + iE_{ex}\,\mathrm{sgn}\,\omega_n}{\pi k_B T_{cS}}},$$

and

$$A_S = k_S\xi_S\tanh\left(k_S d_S/2\right), \quad k_S = \frac{1}{\xi_S}\sqrt{\frac{\omega_n}{\pi k_B T_{cS}}}. \tag{10}$$

Here, E_{ex} is the exchange energy in the ferromagnet. Practically, only the real root of Ω_0 is taken into account, and all imaginary roots are neglected.

The manifestation of proximity effect between F and S is determined by the potential barrier at the interface accounting for the lattice mismatches, interface imperfection, the difference in Fermi velocities, and band structures, etc. The interfacial transparency T_{tran} denotes the projection of the Fermi wave vector onto the direction perpendicular to the interface in the free electron model [17]. In this model, T_{tran} is defined as a parameter for describing the resistance encountered by the electron across the barrier between two metals and is given by

$$\gamma_b = \frac{2}{3}\frac{\ell_F}{\xi_F^*}\frac{1 - T_{tran}}{T_{tran}} = \frac{AR_b}{\rho_F\xi_F^*}. \tag{11}$$

ρ_F is the low temperature residual resistivity of F. R_b is the normal state resistance of the F/S boundary. Thus, the interfacial transparency parameter γ_b in equation (11) is proportional to the interface resistance per unit area, when the superconductor is in the normal state. It is worth to note that the interfacial resistance alone does not dictate the interfacial transparency. It is the ratio of interface resistance to the resistivity of the ferromagnet that is crucial to the interfacial transparency. The behavior of $T_c(d_F)$ can be classified into three regimes according to the values of γ_b: 1) T_c decays nonmonotonically at a finite interface resistance; 2) T_c exhibits reentrant behavior at moderate interface resistance; 3) T_c decays monotonically at low-enough interface resistance. In practice, the value of γ_b is often deduced from the fitting result because of the difficulty in directly measuring the interface resistance. Conventional transport measurement with the current in the plane provides direct access to the critical current and critical magnetic field in the F/S system by driving the S to the normal state. Unfortunately, it gives zero resistance in this configuration when the S is in the superconducting state. The current perpendicular to the plane measurement discussed in the previous section has been proved to be a remarkable method that can provide information about the interface resistance which is inaccessible to the CIP configuration. The corresponding interfacial transparency parameter for $Cu_{0.5}Ni_{0.5}/Nb$ is directly determined to be $\gamma_b = \frac{AR_b}{\rho_F\xi_F^*} \approx 0.2$. The values of systems alike obtained by fitting proximity theory to the $T_c(d_F)$ data agree quantitatively well with this one. They are $\gamma_b = 0.3$ for Nb (11 nm)/$Cu_{0.43}Ni_{0.57}$ bilayers [15],

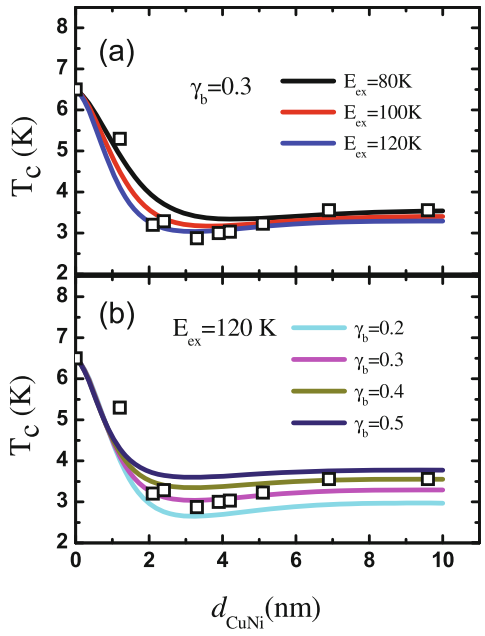

Fig. 5. (Color online) Superconducting critical temperature versus $Cu_{0.5}Ni_{0.5}$ thickness for $Cu_{0.5}Ni_{0.5}$/Nb/$Cu_{0.5}Ni_{0.5}$ trilayers with constant Nb thickness $d_{Nb} = 37$ nm. (a) The solid lines are the fitting results for different values of E_{ex} and fixed $\gamma_b = 0.3$. (b) The solid lines are the fitting results for different values of γ_b and fixed $E_{ex} = 120$ K.

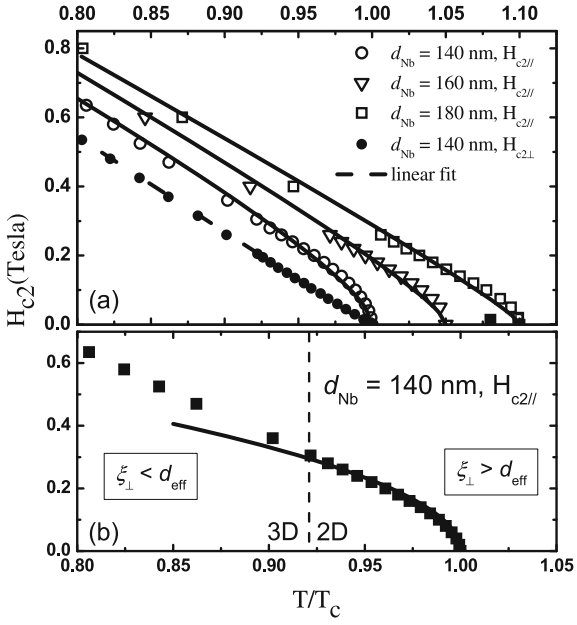

Fig. 6. (a) Reduced parallel upper critical fields versus reduced temperature for $Cu_{0.5}Ni_{0.5}$/Nb multilayers with $d_{Nb} = 140$, 160, and 180 nm. Data of $d_{Nb} = 160$ and 180 nm are shifted to the right by $T/T_c = 0.05$ and 0.1, respectively, for clarity. The solid lines represent the results of the least squares fit using the Ginzburg-Landau relation. The filled circles denote perpendicular upper critical fields for $d_{Nb} = 140$ nm and the dashed line is obtained by a linear fit to the data. (b) The parallel upper critical fields as a function of the reduced temperature for the $Cu_{0.5}Ni_{0.5}$/Nb multilayers with $d_{Nb} = 140$ nm. It can be separated into two sections corresponding to the 3D and 2D behaviors. The latter is indicated by the solid line fitted by the Tinkham's expression [50].

$\gamma_b = 0.57$ for Nb (22.5 nm)/$Cu_{0.4}Ni_{0.6}$ bilayers [19], and $\gamma_b = 0.6$ for CuNi/Nb(23 nm)/CuNi trilayers [13]. However, it is smaller than $\gamma_b = 1.5 \pm 0.3$ for the Nb/$Cu_{1-x}Ni_x$ bilayers with $x = 0.54$ and 0.58 [46] obtained by fitting and $\gamma_b = 1.7$ [21] and $\gamma_b = 2.0$ [47] for Co/Nb and Ni/Nb multilayer with strong ferromagnet, respectively, from CPP measurements.

For comparison, we also deduced the γ_b from the fitting procedure to $T_c(d_F)$ curves. The results fitted by our modified trilayer model are shown in Figure 5. Except for ξ_F^*, which was calculated by equation (9), all other relevant quantities could be derived. The result of $\xi_F^* = 6$ nm is consistent with the values for the Ni composition of both 0.54 and 0.58 in the literature [46]. The exchange energy and the interfacial transparency parameter are used as free parameters in the fitting. Notice that we proceed with the data of $T_c(d_{CuNi})$ first and use the resulting parameters to describe the behavior of $T_c(d_S)$. For a single 37-nm-thick Nb film, T_c is 6.5 K, and the resistivity is about 300 nΩ m at 10 K. The T_c is around 3.5 K for the asymptote of CuNi thickness. It is a little larger than the fitting curve as the star symbol in Figure 6. We suggest this may be due to the uncertainty of T_c to the preparation condition from run to run and the thickness variation about 10% checked by stylus profiler. The Nb coherence length, which is related to the Ginzburg-Landau (GL) coherence length, $\xi_{GL}(0)$, can be determined by the upper critical field measurement as will be discussed in Section 5. From $\xi_{GL}(T) = \pi/2\xi_S(1 - T/T_c)^{-1/2}$, we obtained $\xi_S = 7$ nm.

As can be seen in Figures 5a and 5b, the fittings are more sensitive to the value of γ_b than to that of E_{ex}. The value of E_{ex} is determined mostly in the regime that T_c starts to saturate with respect to d_{CuNi}, whereas that of γ_b is used to distinguish the vertical shift of T_c. The optimal value of E_{ex} in terms of temperature for the fitting is between 80 K and 120 K and that of γ_b between 0.2 and 0.4. If we assume $E_{ex} = k_B T_{Curie}$, then the value of E_{ex} is in agreement with the measurement of T_{Curie} in the single $Cu_{0.5}Ni_{0.5}$ films, as seen in Figure 1. The nonmonotonic behavior of $T_c(d_F)$ exhibits a minimum T_c around $d_{CuNi} = 3.3$ nm. The occurrence of a minimum of $T_c(d_F)$ can be qualitatively explained by the interference of quasiparticle wavefunctions in the F layer, which can be either constructive or destructive depending on the value of d_F. According to Fominov et al. [15], ξ_F^{dirty} is related to the minimum of $T_c(d_F)$ by $d_{min} \approx 0.7\pi\xi_F^{dirty}/2$, where d_{min} is the thickness corresponding to the minimum of $T_c(d_F)$. Moreover, ξ_F^{dirty} denotes the actual decay length of the superconducting Cooper pairs in the F. Notice that ξ_F^{dirty} should not be confused with ξ_F^*, for the latter is associated with the superconducting diffusion length in the normal metal. Using the value of d_{min} extracted from Figure 5, we obtained $\xi_F^{dirty} \approx 3.0$ nm $< \xi_F^*$ as expected, since ξ_F^{dirty} is inversely proportional to the square root of the Curie temperature through the exchange energy

whereas ξ_F^* is inversely proportional to that of the superconducting transition temperature.

The behavior of $T_c(d_S)$ can be characterized with the same set of equations that describes the behavior of $T_c(d_F)$. Here, the dependence of critical temperature on the thickness of a single Nb layer is considered. In Figure 2, the dotted lines are given by the model calculation with fixed parameters $T_{cS} = 8.8$ K, $\rho_{\rm Nb} = 80$ nΩ m, and $\rho_{\rm CuNi} = 300$ nΩ m, whereas the values of γ_b, ξ_F^*, and E_{ex} are taken from the $T_c(d_F)$ fit of Figure 5b. As can be clearly seen, all calculated curves are able to reproduce the experimental data and are comparable to the Radovic's model with the perfect transparency assumption. Despite consistency between the theory and the experimental data, we notice that the effect of a small variation of γ_b is barely distinguishable in the behavior of $T_c(d_S)$. As a result, the behavior of $T_c(d_F)$ should be the key that enables a theoretically quantitative investigation of the interfacial transparency regarding the F/S proximity effect.

According to Angrisani et al., the critical thickness was around 10 nm for Nb/$Cu_{0.46}Ni_{0.54}$ bilayers as a function of dNb with $d$$Cu_{0.46}Ni_{0.54} = 30$ nm, which suggested about 20 nm for trilayer system, and $\gamma_b = 1.5$ for bilayers as a function of dCuNi with dNb = 30 nm [46]. Zdravkov et al. reported that d_{crit} was around 7 nm from $T_c(d_S)$, which gave about 14 nm corresponding d_{crit} with trilayer system, and γ_b was 1.6 from $T_c(d$CuNi) in $Cu_{0.41}Ni_{0.59}$/Nb bilayers wedgelike sample [10]. The critical thickness of 35 nm obtained in our CuNi/Nb/CuNi trilayers was observably large with dCuNi = 50 nm. Aarts et al. were the first to discuss the importance of interface transparency and to present experimental evidence of the intrinsically reduced interface transparency in the $V/V_{1-x}Fe_x$ multilayer system [17]. Their results showed that, for a fixed γ, the critical thickness increases as γ_b decreases. Our value $d_{crit}/\xi_S \sim 5$ with the γ of order of 1 is close to the Aart's calculation limit of about 6 with extremely high transparency. Accordingly, $\gamma_b < 0.4$ obtained for the $Cu_{0.5}Ni_{0.5}$/Nb structure studied in this work reveals a small potential barrier, leading to relatively strong pair-breaking and, thus, a larger critical thickness. This factor of high interfacial transparency derived from the model of microscopic proximity effect is in agreement with the CPP measurement.

5 H_{c2} measurement

We also investigate the influence of interfacial transparency on the temperature-dependent upper critical magnetic field $H_{c2}(T)$ for F/S multilayers. The study of H_{c2} provides information on the coherence length and the role of the pair-breaking effect from the occurrence of the dimensionality crossover. The samples consist of 6 bilayers with fixed $d_F = 20$ nm and various d_S from 50 to 600 nm, denoted as [$Cu_{0.5}Ni_{0.5}$ (20 nm)/Nb(d_S)]$_6$/$Cu_{0.5}Ni_{0.5}$ (20 nm). The d_F-dependent critical field oscillation arising from the different phases between the two adjacent superconductors can be neglected when $d_S/\xi_S > 2$ [48]. The thickness of our samples is well within this regime. Thus, we can compare the results in terms of the barrier quality and exchange energy of the F layer for different samples.

According to the Ginzburg-Landau (GL) theory, the temperature dependence of the perpendicular critical field, $H_{c2\perp}(T)$, always exhibits a linear relationship [49] irrespective of the superconducting thickness, as the one plotted in Figure 6a. The GL coherence length at zero temperature is about 11 nm in our sample, which is obtained from the relationship $\xi_{GL}(0) = \sqrt{\phi_0/2\pi Z T_c}$, where ϕ_0 is the flux quantum and the slope $z = -dH_{c2}/dT$ is deduced from the $H_{c2\perp}(T)$ curves by a linear least squares fit, as the dashed line shown in Figure 6a. On the other hand, the behavior of the temperature dependent parallel critical field, $H_{c2\parallel}(T)$, would change from 3D to 2D when the thickness of the S film is continuously reduced. In the 2D regime, $\xi_\perp(T)$ is limited by the layer thickness, and $H_{c2\parallel}(T)$ shows a square-root-like behavior given by the Tinkham's expression [50]. The temperature dependent $H_{c2\parallel}(T)$ for $Cu_{0.5}Ni_{0.5}$/Nb multilayers with various thicknesses of $d_{\rm Nb} = 140$, 160, and 180 nm are shown in Figure 6. The data for $d_{\rm Nb} = 160$ and 180 nm are shifted to the right by 0.05 and 0.1, respectively, for clarity.

To study the 2D-3D crossover behavior, $H_{c2\parallel}(T)$ data were fitted by $H_{c2\parallel}(T) = a\sqrt{1 - T/T_c} + b(1 - T/T_c)$, as solid lines in Figure 6a. A gradual transition from 2D to 3D was clearly seen evolving from square root behavior to a linear one, when d_S increased from 140 nm to 180 nm. In comparison with the strong ferromagnetic cases reported earlier, the thickness of the 2D to 3D crossover takes place at 145−180 nm in the Nb/Co, and 100−140 nm in the Nb/Fe layered structures [28]. We attribute the comparable dimensional crossover thickness for this relatively weak ferromagnet to the high interfacial transparency between Nb and $Cu_{0.5}Ni_{0.5}$. The influence of transparency on H_{c2} behavior was similar to earlier reports in which the dimensional crossover temperature was shifted toward a lower value in the system exhibiting high interfacial transparency [46,51]. When the magnetic field was applied parallel to the interface, the Cooper pairs moved across the interface and experienced the influence of the interface transparency much more strongly. Since the coherence length $\xi_{GL}(T)$ has $(1 - T/T_c)^{-1/2}$ dependence, $H_{c2\parallel}(T)$ behaves like a 3D system at low temperatures due to $\xi_\perp(T) < d_{\rm Nb}$. However, $\xi_\perp(T)$ tends to diverge when the temperature is sufficiently close to T_c, causing $\xi_\perp(T) > d_{\rm Nb}$, and 2D behavior is observed [46]. In Figure 6b, $H_{c2\parallel}(T)$ for $d_{\rm Nb} = 140$ nm at higher temperatures is well described by a GL square-root fit down to $T/T_c = 0.92$, whereas at lower temperatures $H_{c2\parallel}(T)$ exhibits linear behavior. This result can be regarded as single superconducting films had smaller effective thickness $d_{eff} = 96$ nm estimated by $d_{eff} \approx \xi_\perp(T)$, where the superconductivity of Nb is weakened through the pair-breaking effect at the F/S interface. Consequently, with the introduction of the pair-breaking ratio $\chi = (d_S - d_{eff})/d_{eff}$, the values of χ in different systems are calculated to be

$\chi_{Co} = 0.31$, $\chi_{Fe} = 0.28$, and $\chi_{CuNi} = 0.34$ for comparison. Comparable values of χ regardless of the thickness in the 2D regime confirm that the higher the transparency of the barrier, the stronger its pair-breaking effect would be. This is also consistent with the results of the T_C and CPP measurement discussed in the previous sections.

6 Summary

In summary, we have demonstrated the direct determination of the interfacial transparency of the $Cu_{0.5}Ni_{0.5}$/Nb layered structures and investigated the influence of interfacial transparency on the critical temperature and the upper critical magnetic field. The employment of CPP measurement on the study of interface resistance along with the study of thickness dependent superconducting critical temperature have led to the realization of direct determination of the interfacial transparency between a superconductor and a ferromagnet. The interface resistance is deduced from the best global fit of the one-band model to the unit area resistance which increases linearly with the increasing of the number of the bilayers in both the normal and the superconducting states. $Cu_{0.5}Ni_{0.5}$/Nb layered structures studied in this work are found to have a rather high interfacial transparency ($\gamma_b = 0.2$). This high interfacial transparency results in a strong pair-breaking effect, leading to a relatively large superconducting critical thickness ($d_{crit} = 35$ nm) from the viewpoint of $Cu_{0.5}Ni_{0.5}$ being a weak ferromagnet. Moreover, the results of the temperature dependent upper critical magnetic field reveal that the high interfacial transparency also has a strong influence on the thickness range in which the 2D to 3D crossover takes place. Our results on interfacial transparency can provide important and useful information for the understanding of proximity effect and might even be relevant for the spintronic and/or electronic devices containing F/S heterostructures.

We would like to thank C. Attanasio for his insightful discussions. The financial supports of the National Science Council and the Academia Sinica of Taiwan, Republic of China are acknowledged.

References

1. A.I. Buzdin, Rev. Mod. Phys. **77**, 935 (2005)
2. P. Fulde, R.A. Ferrell, Phys. Rev. **135**, A550 (1964)
3. A.I. Larkin, Y.N. Ovchinnikov, Sov. Phys. JETP. **20**, 762 (1965)
4. J.S. Jiang, D. Davidović, D.H. Reich, C.L. Chien, Phys. Rev. Lett. **74**, 314 (1995)
5. I.A. Garifullin, J. Magn. Magn. Mater. **240**, 571 (2002)
6. V.V. Ryazanov, V.A. Oboznov, A.Yu. Rusanov, A.V. Veretennikov, A.A. Golubov, J. Aarts, Phys. Rev. Lett. **86**, 2427 (2001)
7. V.A. Oboznov, V.V. Bol'ginov, A.K. Feofanov, V.V. Ryazanov, A.I. Buzdin, Phys. Rev. Lett. **96**, 197003 (2006)
8. J.W.A. Robinson, S. Piano, G. Burnell, C. Bell, M.G. Blamire, Phys. Rev. B **76**, 094522 (2007)
9. I.A. Garifullin, D.A. Tikhonov, N.N. Garif'yanov, L. Lazar, Yu.V. Goryunov, S.Ya. Khlebnikov, L.R. Tagirov, K. Westerholt, H. Zabel, Phys. Rev. B **66**, 020505(R) (2002)
10. V. Zdravkov, A. Sidorenko, G. Obermeier, S. Gsell, M. Schreck, C. Müller, S. Horn, R. Tidecks, L.R. Tagirov, Phys. Rev. Lett. **97**, 057004 (2006)
11. L.R. Tagirov, Phys. Rev. Lett. **83**, 2058 (1999)
12. J.Y. Gu, C.-Y. You, J.S. Jiang, J. Pearson, Ya.B. Bazaliy, S.D. Bader, Phys. Rev. Lett. **89**, 267001 (2002)
13. A. Potenza, C.H. Marrows, Phys. Rev. B **71**, 180503(R) (2005)
14. L.R. Tagirov, Physica C **307**, 145 (1998)
15. Ya.V. Fominov, N.M. Chtchelkatchev, A.A. Golubov, Phys. Rev. B **66**, 014507 (2002)
16. R. Gross, A. Sidorenko, L. Tragirov, *Nanoscale Devices-Fundamentals and Applications* (Springer, 2004)
17. J. Aarts, J.M.E. Geers, E. Bruck, A.A. Golubov, R. Coehoorn, Phys. Rev. B **56**, 2779 (1997)
18. C. Cirillo, S.L. Prischepa, M. Salvato, C. Attanasio, M. Hesselberth, J. Aarts, Phys. Rev. B **72**, 144511 (2005)
19. J. Kim, Jun Hyung Kwon, K. Char, Hyeonjin Doh, Han-Yong Choi, Phys. Rev. B **72**, 014518 (2005)
20. J. Kim, Y.-J. Doh, K. Char, Phys. Rev. B **71**, 214519 (2005)
21. S.Y. Huang, S.F. Lee, S.Y. Hsu, Y.D. Yao, Phys. Rev. B **76**, 024521 (2007)
22. C.G. Robbins, H. Claus, P.A. Beck, Phys. Rev. Lett. **22**, 1307 (1969)
23. K. Levin, D.L. Mills, Phys. Rev. B **9**, 2354 (1974)
24. J.W. Loram, Z. Chen, J. Phys. F: Met. Phys. **13**, 1519 (1983)
25. Z. Radović, M. Ledvij, L. Dobrosavljević-Grujić, A.I. Buzdin, J.R. Clem, Phys. Rev. B **44**, 759 (1991)
26. S.Y. Huang, J.J. Liang, T.C. Tsai, L.K. Lin, M.S. Lin, S.Y. Hsu, S.F. Lee, J. Appl. Phys. **103**, 07c704 (2008)
27. J.J. Liang, S.F. Lee, W.T. Shih, W.L. Chang, C. Yu, Y.D. Yao, J. Appl. Phys. **92**, 2624 (2002)
28. S.Y. Huang, S.F. Lee, J.J. Liang, C.Y. Yu, K.L. You, T.W. Chiang, S.Y. Hsu, Y.D. Yao, J. Magn. Magn. Mater. **304**, e81 (2006)
29. A.S. Sidorenko, V.I. Zdravkov, J. Kehrle, R. Morari, G. Obermeier, S. Gsell, M. Schreck, C. Muller, M.Yu. Kupriyanov, V.V. Ryazanov, S. Horn, L.R. Tagirov, R. Tidecks, JETP Lett. **90**, 139 (2009)
30. A. Rusanov, R. Boogaard, M. Hesselberth, H. Sellier, J. Aarts, Pyhsica C **369**, 300 (2002)
31. H. Zabel, S.D Bader, *Magnetic Heterostructures: Advances and Perspectives in Spinstructures and Spintransport* (Springer Tracts in Modern Physics, 2007), p. 251
32. F. Taddei, S. Sanvito, J.H. Jefferson, C.J. Lambert, Phys. Rev. Lett. **82**, 4938 (1999)
33. K. Eid, H. Kurt, W.P. Pratt, Jr, J. Bass, Phys. Rev. B **70**, 100411(R) (2004)
34. S.F. Lee, S.Y. Huang, J.H. Kuo, Y.A. Lin, L.K. Lin, Y.D. Yao, J. Appl. Phys. **93**, 8212 (2003)
35. P. Cadden-Zimansky, Ya.B. Bazaliy, L.M. Litvak, J.S. Jiang, J. Pearson, J.Y. Gu, Chun-Yeol You, M.R. Beasley, S.D. Bader, Phys. Rev. B **77**, 18450 (2008)

36. R.S. Keizer, S.T.B. Goennenwein, T.M. Klapwijk, G. Miao, G. Xiao, A. Gupta, Nature (London) **439**, 825 (2006)
37. F.S. Bergeret, A.F. Volkov, K.B. Efetov, Phys. Rev. Lett. **86**, 4096 (2001)
38. A. Kadigrobov, R.I. Shekhter, M. Jonson, Europhys. Lett. **54**, 394 (2001)
39. I.S. Veshchunov et al., JETP Lett. **88**, 758 (2008)
40. T.S. Khaire, M.A. Khasawneh, W.P. Pratt, Jr, N.O. Birge, Phys. Rev. Lett. **104**, 137002 (2010)
41. C. Fierz, S.F. Lee, J. Bass, W.P. Pratt Jr, P.A. Schroeder, J. Phys. Cond. Matter **2**, 9701 (1990)
42. S.F. Lee, Q. Yang, P. Holody, R. Loloee, J.H. Hetherington, S. Mahmood, B. Ikegami, K. Vigen, L.L. Henry, P.A. Schroeder, W.P. Pratt Jr, J. Bass, Phys. Rev. B **52**, 15426 (1995)
43. G.E. Blonder, M. Tinkham, T.M. Klapwijk, Phys. Rev. B **25**, 4515 (1982)
44. S. Takahashi, S. Maekawa, J. Phy. Soc. Jpn **77**, 031009 (2008)
45. M.Yu. Kuprianov, V.F. Lukichev, Sov. Phys. JETP **67**, 1163 (1988)
46. A. Angrisani Armenio, C. Cirillo, G. Iannone, S.L. Prischepa, C. Attanasio, Phys. Rev. B **76**, 024515 (2007)
47. S.Y. Huang, Y.C. Chiu, J.J. Liang, L.K. Lin, T.C. Tsai, S.Y. Hsu, S.F. Lee, J. Appl. Phys. **105**, 07E319 (2009)
48. B. Krunavakarn, S. Yoksan, Physica C **440**, 25 (2006)
49. S.F. Lee, T.M. Chuang, S.Y. Huang, W.L. Chang, Y.D. Yao, J. Appl. Phys. **89**, 7493 (2001)
50. M. Tinkham, *Introduction to Superconductivity* (McGraw-Hill, New York, 1975)
51. C. Ciuhu, A. Lodder, Phys. Rev. B **64**, 224526 (2001)